Ultrafine-Grained Laminated Metal Composites: A New Material Class for Tailoring Cyclically Stressed Components

Frank Kümmel,* Heinz Werner Höppel, and Mathias Göken

The service life of technical components is often limited by the fatigue strength of the deployed materials. The accumulative roll bonding (ARB) process, which has the ability to produce ultrafine-grained (UFG) laminated metal composites with tailored properties, offers a unique method to significantly enhance the fatigue life of materials that are cyclically loaded in three-point bending. Detailed microstructural investigations reveal the material- and load-specific deformation and damage mechanisms. Composites that have a sufficiently high difference in strength between the different constituent layers exhibit a significantly impeded crack growth and therefore an extended fatigue life at high stress amplitudes compared with those laminates with a rather similar strength of the different constituents. In the former composites, the fatigue crack is deflected at the material interface as it propagates from the softer to the harder layer. At low stress amplitudes, a prolonged fatigue life of the composites is mainly because of a significantly increased resistance to crack initiation. On the one side, this is as a result of the introduction of an UFG microstructure. On the other side, a load transfer toward stiffer layers in the interior of the composites also accounts for the enhanced fatigue life, if elastically dissimilar materials are combined in the right manner.

1. Introduction

Technical components are frequently exposed to cyclic loads. These cyclic stresses are often very small but can result in a severe failure of the material, although the applied stress amplitudes are significantly smaller than the yield value of the material. The phenomenon of material fatigue has been systematically investigated since the nineteenth century.[1,2] Nowadays, cyclically loaded parts are increasingly governed by new light-weight design concepts. Thus, new materials with a high-specific monotonic and cyclic strength come into play. For the prospective use of new light-weight material concepts in engineering applications, it is extremely important to understand the damage mechanisms that occur during cyclic loading in detail. Different approaches to enhance the fatigue life in aluminum-based materials that are cyclically are discussed in the following:

One approach to enhance the fatigue life of materials is by increasing the strength of the material. This is often achieved by alloying.[3–6] However, one major drawback is that the corrosion properties often get worse in the higher alloyed systems, compared with less or unalloyed samples.[7] Another method to enhance the strength is given by grain refinement. The advantage of this method is that the increase in strength is achieved without changing the chemical composition of the material. Particularly effective methods to reduce the grain size up to the submicrometer range are the severe plastic deformation processes.[8–10] The materials are subjected to high plastic deformation without changing the cross-sectional shape of the material during these processes. It is possible to introduce a very high amount of plastic deformation and therefore also new dislocations into the material by repeating the process steps several times. These dislocations form new subgrains which transform by further deformation into high-angle grain boundaries as a result of energetic minimization. The cyclic properties of such ultrafine-grained (UFG) materials are significantly better in comparison with their coarse-grained (CG) counterparts.[10–13] The development of dislocation arrangements and/or structures that typically accommodate strain during fatigue in CG materials is hindered because of the small grain size in UFG materials.[14,15]

Another highly interesting method to enhance the fatigue properties is to combine different materials, both in terms of mechanical strength, as well as Young's modulus, to laminated metal composites (LMCs). Fundamental research has been

Dr. F. Kümmel, Dr. H. W. Höppel, Prof. M. Göken
Materials Science & Engineering
Friedrich-Alexander-Universität Erlangen-Nürnberg (FAU)
Institute 1
Martensstr. 5, Erlangen 91058, Germany
E-mail: frank.kuemmel@frm2.tum.de

Dr. F. Kümmel
Heinz Maier-Leibnitz Zentrum (MLZ)
TU München
Lichtenbergstr. 1, Garching 85748, Germany

The ORCID identification number(s) for the author(s) of this article can be found under https://doi.org/10.1002/adem.202100070.

carried out by various researchers on the influence of such heterogeneous interfaces on the fatigue properties of LMCs, especially with a focus on the difference in hardness at the material interface.[16–23] The results show that the bifurcation of a fatigue crack in the vicinity of the material interface is the key to prolonged fatigue life, as this results in a reduced crack propagation rate.[20,21] The influence of a difference in the Young's modulus on the cracking behavior has also been previously studied in literature, mainly by different modeling approaches.[24–26] It was elaborated that the near-tip crack-driving force changes at the material interface resulting in shielding or antishielding of the crack tip, if the crack propagates from a material with a lower Young's modulus to a material with a higher one or vice versa.[24] However, a major drawback hindering the widespread use of LMCs has been the high manufacturing costs so far.

With the development of the accumulative roll bonding (ARB),[27] which is one of the most prominent severe plastic deformation processes, a more cost-efficient method has been introduced for the fabrication of LMCs with a high number of heterogeneous interfaces beyond the laboratory scale.[28] This enables the combination of a laminated layered structure together with an UFG microstructure.[29–33] Furthermore, tailored or graded properties can be realized to meet particular requirements, as the ARB process allows the material combination, as well as the layer architecture to be varied.[34–38]

2. Experimental Section

2.1. Processing of the UFG LMCs

In the current work, three different aluminum alloys were used, which vary in the amount of foreign elements (AA1050:Al99.5, AA5005:Al98.6, and AA5754:Al95.9). The chemical composition of the different alloys is shown in **Table 1**. The foreign elements were mainly solutionized in the aluminum matrix in all three aluminum samples. The deep drawing steel DC01 was used for one LMC variant to investigate the influence of a difference in mechanical strength and Young's modulus at the heterogeneous material interface. UFG LMCs, consisting of layers from different materials, and monomaterials, consisting of layers of the same material, were produced by different numbers of ARB cycles. Prior to ARB processing, the sheets were cold rolled from a thickness of 5.0–2.5 mm. Before every ARB cycle, the surfaces were cleaned by acetone and then wire brushed to remove the oxide layer and to ensure a sufficient bonding. Subsequently,
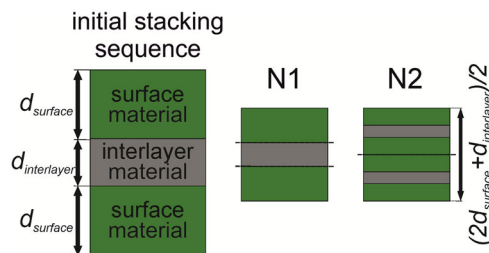
the treated surfaces were stacked on each other and roll bonded at room temperature using a four high rolling mill (BW 300, Carl Wezel, Germany) with a nominal thickness reduction of 50% per ARB cycle. The bonded sheets were air cooled and halved before performing the next ARB cycle. All the samples in this work were produced in a similar manner. The stacking sequences and material combinations used are shown schematically in **Figure 1**. In the first ARB cycle, the thinner sheet of the constituent that has the higher strength/elastic modulus was stacked in between two sheets of the constituents that have the lower strength/elastic modulus. As a result, a symmetric layer architecture already existed from the first ARB cycle, which leads to a more uniform deformation of the sheet. Through a second ARB cycle, a sheet with two interlayers of the stronger constituent was produced. The different LMCs produced are denoted as follows: The base material (e.g., AA1050), which was also the outer layer material, was always indicated first followed by the interlayer material (e.g., AA5005). Thus, the LMCs were then denoted as AA1050/AA5005. As reference material, monomaterial sheets with the same stacking sequence were also produced by up to four ARB cycles.

2.2. Characterization of Microstructure and Local Mechanical Properties

The layer architecture and the microstructure of the LMCs were characterized by scanning electron microscopy (Crossbeam 1540 EsB, Zeiss, Germany) using secondary and backscattered electron contrast techniques. All sheets were analyzed in side view (rolling direction × normal direction). Therefore, the specimens were ground down to a grit size of 6 μm and then mechanically polished up to 1 μm. In the final step, the specimens were polished chemomechanically using an active oxide polishing suspension (OP-S, Struers, Germany). The local mechanical properties were measured by nanoindentation experiments (Nanoindenter XP, MTS Nano Instruments, USA) using a three-sided Berkovich pyramid with the continuous stiffness method.[39] In each sample 40–60 indents were carried out across the layer interface. The indentation fields were positioned at an angle of 30° to the rolling direction to increase the spatial resolution. The indentation depth was 500 nm to minimize the indentation size effect, but also to ensure that the deformation around an indent was constrained within one material. To avoid an influence of the damage zone around an indent, the distance between the indents was always 20-fold the indentation depth.[40]

Table 1. Chemical composition of the aluminum and steel sheets in wt% measured by spark spectrometry.

Alloy	Chemical composition in wt%								Others	
	Al	Mg	Fe	Si	Mn	Cu	Zn	Ti	Each	Total
AA1050	99.4	0.04	0.33	0.11	0.03	0.04	0.01	0.02	<0.02	0.04
AA5005	98.6	0.92	0.25	0.11	0.02	0.02	0.01	0.01	<0.01	0.06
AA5754	95.9	2.86	0.37	0.33	0.30	0.05	0.02	0.04	<0.04	0.13
			Fe	C	Mn	Cu	Al	Si	Each	Total
DC01	–	–	99.50	0.06	0.20	0.06	0.05	0.03	<0.02	0.10

Figure 1. Schematic illustration of the processing of the different LMCs and monomaterial samples. The bonded surfaces are indicated by the dashed black lines in each ARB cycle.

2.3. Determination of the Cyclic Mechanical Properties

The fatigue tests were carried out on a vibrophore testing machine (HFP 5100, Roell Amsler, Germany) in three-point-bending mode at a frequency of around 70 Hz, which resulted in strain rates in the order of $10^{-1}\,s^{-1}$. All tests were conducted under force control with a stress ratio R of 0.1, leading to a mean tensile stress in the lower part of the sample. Furthermore, a measurement of the test frequency during fatigue enabled the determination of the number of fatigue cycles for macrocrack nucleation and propagation. As the frequency of the tests depends on the stiffness of the sample, a frequency drop is correlated to the propagating macrocrack. After fatigue testing, the crack path was analyzed by scanning electron microscopy in secondary electron technique. The two supports and the central loading anvil had a 5 mm diameter and the distance between the two supports was 15 mm. Specimens with dimensions of 20 mm length × 9.5 mm width × 3 mm height were machined out in rolling × transverse × normal direction of the sheet. The specimens were ground down to a grid size of 6 µm mechanically before testing. The maximum bending stress σ_b at the bottom surface in the center of the sample can be calculated with Equation (1), with F being the applied force, L the distance between the supports, b the width, and h the height of the sample.

$$\sigma_b = \frac{3 \cdot F \cdot L}{2 \cdot b \cdot h^2} \tag{1}$$
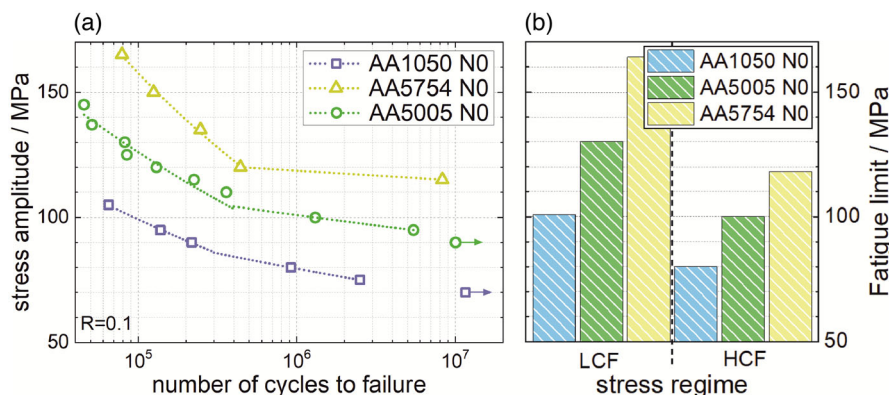
3. Results

3.1. Hardness in CG Materials

In recent years, a widespread and efficient method to enhance the cyclical mechanical properties was to increase the strength of the materials by alloying, especially if the material was loaded in the high cycle regime. Therefore, also in this work, the cyclic mechanical properties of the three different investigated materials were measured in the annealed, CG condition before ARB processing. The hardness of the three different aluminum
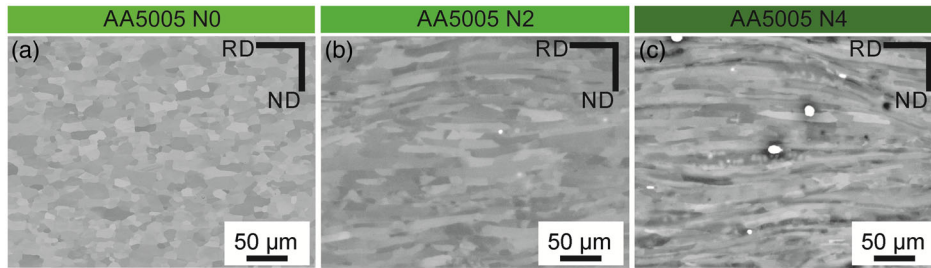
samples rises with an increasing amount of foreign elements from AA1050 (0.56 GPa) to AA5005 (0.79 GPa) to AA5754 (0.83 GPa). The results of the fatigue tests are shown in a Wöhler S–N diagram, **Figure 2**a, where the maximum stress amplitude at the bottom of the sample is plotted against the logarithmic number of fatigue cycles to failure. The fatigue life curves of all monomaterials can clearly be separated into the low cycle fatigue (LCF) and high cycle fatigue (HCF) regimes at a threshold stress $\sigma_{threshold}$. At this point, the mean stress during fatigue exceeds the yield strength of the material. Therefore, at higher stresses than $\sigma_{threshold}$, pronounced plastic deformation of the lower part of the sample takes place. The fraction of macrocrack propagation on the total fatigue life discernably differs between these two stages for the monomaterials. The macrocrack begins to propagate at 95% of the total fatigue life ($N_{propagation} \approx 5\%\ N_{failure}$) for all monomaterials, if the stress amplitudes lies above $\sigma_{threshold}$. If the maximum stress amplitudes are below $\sigma_{threshold}$, the fatigue life is almost entirely governed by the initiation of the macrocrack for all monomaterials ($N_{propagation} \approx 1\%\ N_{failure}$). The increasing hardness of the materials clearly shifts the fatigue life curves of the materials to higher stress amplitudes. Figure 2b shows the endurable stress amplitudes (fatigue limit) at 8×10^4 cycles for the LCF regime, and at 2×10^6 cycles for HCF regime, are plotted. The fatigue life in both regimes is significantly enhanced with the increasing amount of alloying elements. Similar results have already been found by Höppel et al.[41] for Al–Mg alloys tested under uniaxial fatigue loading.

3.2. UFG Microstructure

Another method to enhance the strength of materials is by reducing the grain size. **Figure 3** shows the microstructure after different numbers of ARB cycles (N0, N2, and N4) are depicted exemplarily for AA5005. The AA1050 and AA5754 samples display a very similar behavior both regarding the grain refinement process, as well as the mechanical properties. The grain size is clearly reduced and a very homogenous UFG structure is already achieved after two ARB cycles. This is due to the cold rolling of the sheets prior to ARB, leading to a high dislocation density and

Figure 2. Influence of an increasing alloying content on the fatigue life shown in a) fatigue life diagram (S–N curve) and in b) the endurable stress amplitudes (fatigue limit) at 8×10^4 or, respectively, 2×10^6 fatigue cycles to failure, that are representative for the fatigue life in the LCF and HCF regimes are plotted.

Figure 3. Microstructure of AA5005 after different numbers of ARB cycles a) before processing (N0), b) after two ARB cycles (N2), and c) after four ARB cycles (N4).
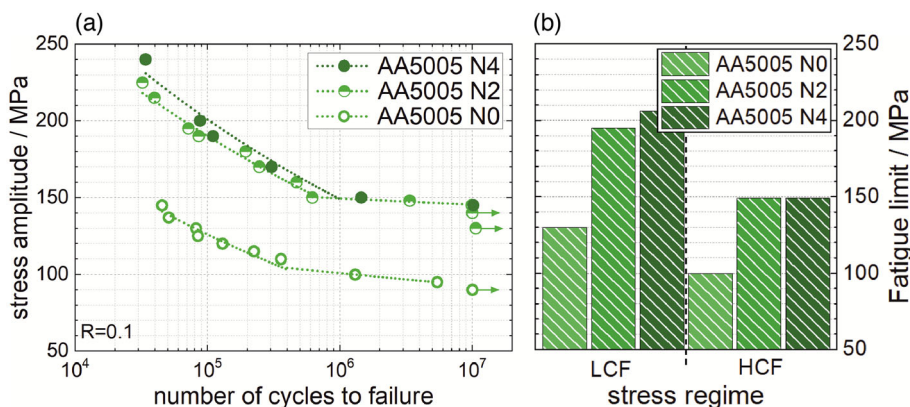
thus accelerating the grain refinement process in the following ARB cycles. The grain refinement between the 2nd and 4th ARB cycle is not as strongly pronounced, which is in good accordance with literature:[42–44] The major part of grain refinement takes place during the first ARB cycle. After a given number of ARB cycles, a quasistationary saturation grain size is developed as a result of a compensatory effect of dislocation generation and annihilation. In this regime further ARB cycles mainly increase the misorientation between the grains.[45]

The decreasing grain size evidently influences the mechanical properties of the material: The hardness rises with an increasing number of ARB cycles from the annealed pre-ARB state (N0: 0.79 GPa) to the sample after ARB processing (N2: 1.12 GPa and N4: 1.32 GPa). Fatigue life is also significantly improved between the first two ARB cycles, at which most of the grain refinement takes place, **Figure 4**. The fatigue life curve of the N2 sample is considerably shifted to higher stress amplitudes compared with the N0 sample, Figure 4a. In contrast, the fatigue life of the N4 sample is only slightly increased in the LCF regime and almost identical in the HCF regime compared with the N2 sample. Figure 4b shows the influence of an increasing number of ARB cycles on the endurable stress amplitudes at 5×10^4 and 5×10^6 cycles is shown. The first two ARB cycles lead to a strong increase in fatigue life both in the LCF and the HCF regimes. In between the 2nd and 4th ARB cycle, the fatigue life is slightly increased in the LCF regime.

The fatigue life of the monomaterial samples is mainly dominated by the initiation of a macrocrack for all stress amplitudes investigated and for all differently ARB-processed conditions. However, the fraction of macrocrack propagation on the total fatigue life is significantly higher in the LCF regime ($N_{propagation} \approx 8\%$ $N_{failure}$) compared with the HCF regime ($N_{propagation} \approx 1\%$ $N_{failure}$). Therefore, the microstructural changes in between the 2nd and 4th ARB cycle mainly influence the crack propagation in the samples.

3.3. Homogenous LMCs: Aluminum/Aluminum LMCs

In addition to the development of an UFG microstructure, it is also possible to produce LMCs by the ARB process. In this context, we have to discern between homogenous and heterogeneous LMCs. In the first case, the LMC consists of layer materials that all belong to the same alloy family, for example, aluminum alloys. In the latter one, the layer materials belong to different alloy families, for example, aluminum alloys combined with steel. In this section, the influence of homogenous LMCs that are made of the different aluminum alloys AA1050/AA5005 and AA1050/AA5754 is discussed. In these LMCs, only a difference in hardness is present at the material interface. The difference in elastic properties is rather small and can be neglected. A 1.5 mm-thick sheet of the harder material (AA5005 or AA5754) was roll-bonded into two 2.5 mm thick
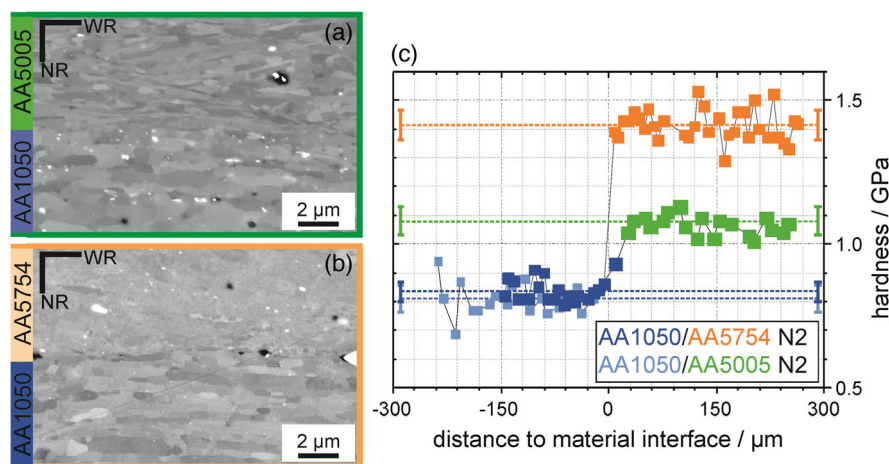

Figure 4. Influence of an increasing number of ARB cycles on the fatigue life shown a) in the fatigue life diagram (*S–N* curve) and b) the endurable stress amplitudes (fatigue limit) at 5×10^4 or, respectively, 5×10^6 fatigue cycles to failure, that are representative for the fatigue life in the LCF and HCF regimes are plotted, exemplarily shown for AA5005. The AA1050 and AA5754 samples showed a very similar behavior. With data from the study by Kümmel et al.[22]

AA1050 sheets in the 1st ARB cycle in both LMCs, resulting in a "sandwich-like" structure. After the second ARB cycle, LMCs consisting of low strength AA1050 layers and of two interlayers of a harder material, either AA5005 or AA5754, are produced. The positions of the interlayers are at ¼ and ¾ of the total height of the samples. The bonding between the two metals is good and no macroscopic bonding defects are visible at the interface. A homogenous layer architecture is achieved in both LMCs without pronounced necking of the harder layer. The microstructure at the material interface is shown in **Figure 5**a,b. The different aluminum alloys can clearly be identified by their different grain sizes. In the AA1050 layers, the grain size is the largest. The grain size in the AA5005 layers is slightly smaller, and in the AA5754 layers, the grain size is considerably reduced. This is related to the higher amount of solute atoms in the alloys.[46] The microstructures in the LMCs and in the corresponding monomaterials are very comparable. Similar observations have been made in a previous study performed on AA1050A/AA5005 LMCs, in which the grain size in the composite is very similar to the one in UFG monomaterials, if the number of ARB cycles and therefore layer interfaces is low.[33]
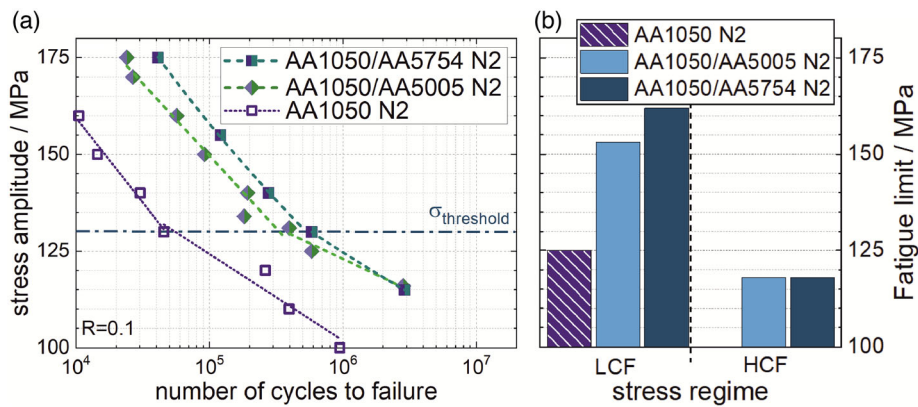
Hardness profiles across the layer interface in the AA1050/AA5005 and AA1050/AA5754 LMCs are shown in Figure 5c. The hardness in all layers is quite homogenous. However, a small increase in the softer layer and decrease in the harder layer in the vicinity of the material interface can be detected. Although the indent is visually in one material, the plastically deformed volume around the indent is already influenced by the adjacent layer, and thus the indentation depth increases and the resulting hardness decreases. To better compare for the overall behavior, the more meaningful values of the mean hardness of the different materials are plotted as dashed lines. The hardness correlates well to the microstructural observations. The lowest hardness is present in the AA1050A layers, a medium one in the AA5005 layers, and the highest one in the AA5754 layers. A comparison of the composites with conventionally ARB-processed monomaterials reveals that the hardness of the individual layers is also very similar. Summarizing, one can conclude that the microstructure and the hardness of the outer layer in the AA1050/

AA5005 and AA1050/AA5754 LMCs and AA1050 monomaterial are identical. The only differences are the hardness differences at the layer interface, which can account for feasible differences in the fatigue life and crack propagation mechanisms.

The fatigue life curves of the AA1050/AA5005 and the AA1050/AA5754 LMCs, as well as the AA1050 monomaterial are shown in **Figure 6**a. The fatigue life curves of both LMCs and the monomaterial can clearly be separated to the LCF and HCF regimes at a threshold stress $\sigma_{threshold(AA1050)}$ of 130 MPa. At this point, the mean stress during fatigue in the sample reaches 150 MPa, which is identical to the yield strength of the AA1050 UFG monomaterial after 2 ARB cycles.[47] Therefore, at stresses higher than $\sigma_{threshold}$, pronounced plastic deformation of the lower part of the sample takes place. At stress amplitudes above $\sigma_{threshold}$, the fraction of macrocrack propagation on the total fatigue life strongly differs between the LMCs and the monomaterial. At these stresses, the macrocrack propagation clearly covers a larger part of the total fatigue life in the LMCs ($N_{propagation} \approx 15\%$ $N_{failure}$) compared with the monomaterial ($N_{propagation} \approx 5\%$ $N_{failure}$). Concurrently, at stress amplitudes below $\sigma_{threshold(AA1050)}$, the fraction of macrocrack propagation is similar for all samples ($N_{propagation} \approx 1–5\%$ $N_{failure}$). Figure 6b shows the endurable stress amplitudes at a) 5×10^4 and b) 1×10^6 fatigue cycles to failure is depicted for the different LMCs and the monomaterial. These values are representative for the fatigue life in the LCF and HCF regimes, respectively. For both LMCs, a considerably improved fatigue life is achieved compared with the monomaterial sheet in the LCF and HCF regimes. Comparing the two LMCs, the fatigue life of both composites is almost identical at stress amplitudes below the threshold stress $\sigma_{threshold}$. However, at higher stress amplitudes, the fatigue life of the AA1050/AA5754 composite is significantly higher. As discussed earlier, there are no microstructural differences between the outer AA1050 layers in the LMCs and the monomaterial. Thus, the differences in the fatigue behavior must be related to the higher hardness gradient at the layer interface. The higher the hardness difference between the constituent materials, the longer the fatigue life.

Figure 5. a,b) Microstructures at the material interfaces and c) hardness profiles across the layer interface for the AA1050/AA5005 and AA1050/AA5754 LMCs. The mean hardness of the individual layers is shown as a dashed line.

**ADVANCED
SCIENCE NEWS**
www.advancedsciencenews.com

**ADVANCED
ENGINEERING
MATERIALS**
www.aem-journal.com

Figure 6. Influence of an increasing hardness difference at the material interface on the fatigue life shown in a) fatigue life diagram (S–N curve) and in b) the endurable stress amplitudes at (fatigue limit) at 5×10^4 and 1×10^6 fatigue cycles to failure that are representative for the fatigue life in the LCF and HCF regimes. With data from the study by Kümmel et al.[22]

3.4. Heterogeneous LMCs: Aluminum/Steel LMCs

In addition to the combination of similar materials, which were discussed in Section 3.3, it is also possible to combine different materials in the ARB process. This enables the material properties to be tailored by varying the differences in strength of the individual layers and also the differences in the Young's modulus at the material interfaces. An aluminum/steel LMC consisting of the aluminum alloy AA5005 and of the deep drawing steel DC01 has been produced to investigate the influence of this heterostructure on the fatigue behavior. A large difference in elastic modulus (AA5005: 70 GPa,[48] DC01: 210 GPa[49]) is present at the material interface in this LMC. The processing of this LMC was similar to the LMCs in the previous sections. In the 1st ARB cycle, a 1 mm-thick sheet of DC01 was roll bonded between two 2.5 mm-thick sheets of A5005 resulting in a "sandwich-like" structure. After the 2nd ARB cycle, a LMC based on aluminum with two steel interlayers is formed. The interlayers are at ¼ and ¾ of the total height of the samples.
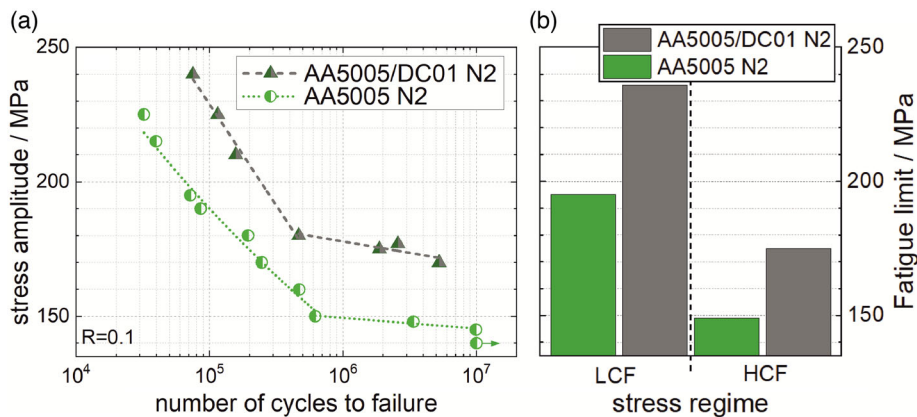
The layer architecture, microstructure, and hardness across the interface of the AA5005/DC01 LMC after the 2nd ARB cycles was already investigated in the study by Kümmel et al.:[50] The layer architecture of the LMC is very uniform. The bonding between the materials is good and there are no macroscopic bonding defects present at the material interface. The mean grain size in both materials is well below 1 μm and is strongly elongated along the rolling direction. The grain size in the AA5005 layers in this LMCs is very similar to that of the AA5005 monomaterial sample, Figure 3. In comparison, the grain size in the DC01 layers is rather inhomogeneous. The microstructure in this layer mainly consists of UFG grains with their typical elongated shape. However, in some areas, equiaxed grains with a diameter of about 1 μm can be found. The hardness is very homogeneous within the AA5005 layers. The hardness of the AA5005 monomaterial is almost the same as in the LMC. The hardness of the DC01 interlayer is significantly higher than that of the AA5005 layers. Furthermore, the hardness in DC01 scatters more strongly as a result of the more inhomogeneous microstructure. The hardness difference of 1.96 GPa at the material

interface is very large, which corresponds to 178% of the hardness of the AA5005 layers. It was demonstrated by finite element simulations in the studies by Kümmel et al.[50,51] that a strong stress localization into the steel layer takes place in the aluminum/steel LMCs. This results in a maximum tensile stress of 135% at the lower steel-aluminum interface compared with the maximum stress in an aluminum monomaterial sample. In contrast to that, the maximum tensile stress in the outer aluminum layer decreases to only 82% of the value obtained for a specimen with a constant Young's modulus (aluminum monomaterial or homogenous Al/Al LMC condition).

The fatigue life of the AA5005/DC01 LMC is significantly increased compared with the AA5005 monomaterial both in the LCF and HCF regimes, **Figure 7**a,b. The increase in fatigue life in the LCF regime is a consequence of an improved resistance against crack propagation. In the AA5005/DC01 LMC a larger part of the total fatigue life is covered by macrocrack propagation ($N_{propagation} \approx 25\%$ $N_{failure}$). As a reminder, this value amounts only to 5% for the monomaterial sample. In the HCF regime, the fatigue lives for all samples are mainly determined by the crack initiation ($N_{propagation} \approx 1–5\%$ $N_{failure}$). The significantly enhanced fatigue limit in the HCF regime ($\approx 20\%$) is mainly due to the stress reduction in the outer AA5005 surface, which is about 18% in the AA5005/DC01 LMC compared with the AA5005 monomaterial.

4. Discussion

The influence of different materials and layered structures, which can be tailored within the ARB process, on the fatigue life of UFG LMCs and monomaterials was investigated under cyclic three-point-bending fatigue in this article. A similar manufacturing process was chosen in all samples to be able to examine only the influence of one parameter. In the 1st ARB cycle, a stronger material (volume fraction about 20%) was roll bonded between two sheets of a softer material. After the 2nd ARB cycle, a LMC with two interlayers made of the stronger material within a softer base material are achieved, Figure 1. The outer layer of the LMC always consists of the softer base material. A distinction was

**ADVANCED
SCIENCE NEWS**

www.advancedsciencenews.com

**ADVANCED
ENGINEERING
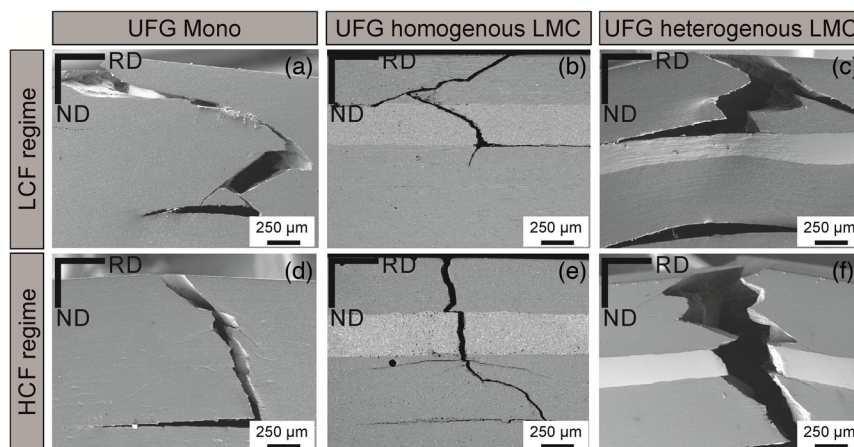MATERIALS**

www.aem-journal.com

Figure 7. Influence of an difference in hardness and Young's Modulus at the material interface on the fatigue life shown a) in a fatigue life diagram (S–N curve) and b) endurable stress amplitudes (fatigue limit) at 8×10^4 and 5×10^6 fatigue cycles to failure that are representatively for the fatigue life in the LCF and HCF regimes. With data from the study by Kümmel et al.[50]

made between homogenous and heterogeneous LMCs, which have been produced from different aluminum alloys or from a combination of an aluminum alloy and a deep drawing steel, respectively. Monomaterials with a similar processing route were also investigated as a reference.
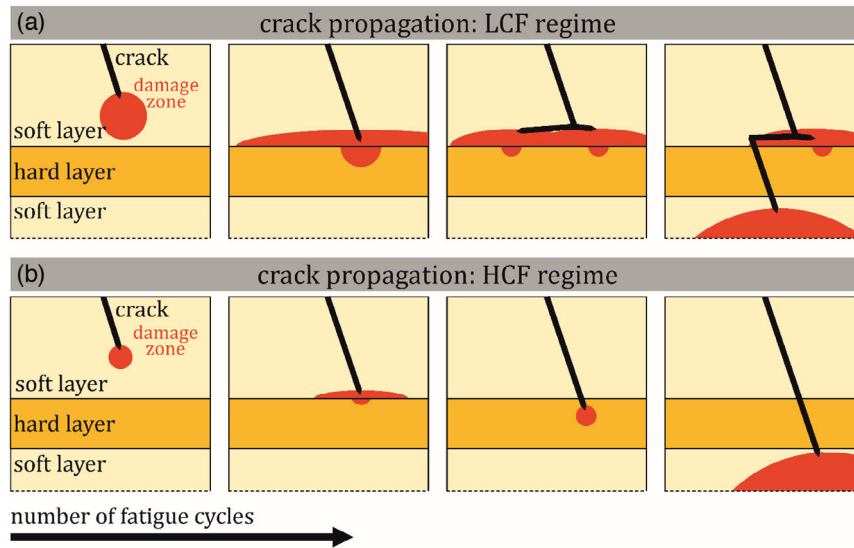
The crack propagation behavior in the LMCs differs fundamentally from the behavior in comparable monomaterials, **Figure 8**. A pronounced crack deflection at the material interface occurs in the LMCs at high stress amplitudes (LCF regime), if a high difference in hardness between the materials exists. The crack propagates further nearly parallel to the stress axis and to the soft-to-hard material interface within the softer layer. This process is much more pronounced in the aluminum/steel LMCs, at which a very high difference in hardness is present at the material interface. The crack deviation leads to a significant retardation of the macrocrack propagation. The fraction of the macrocrack propagation on the total fatigue life increases in the homogenous LMCs ($N_{propagation} \approx 15\%$ $N_{failure}$) to the heterogeneous aluminum/steel LMCs ($N_{propagation} \approx 25\%$ $N_{failure}$) as a result. For comparison, this fraction is only 5% in the aluminum

monomaterial samples. The influence of the difference in hardness is eliminated and the crack propagates very straight across the material interfaces for all LMCs at low stress amplitudes (HCF regime). Thus, the fatigue life in the HCF regime is almost completely determined by the macrocrack initiation in the outer layer ($N_{initiation} \approx 91$–$95\%$ $N_{failure}$).

The deviation in crack paths in between the experiments at high and low stress amplitudes can be explained by the deformation behavior in front of the crack tip. One important parameter to be mentioned here is the stress intensity factor, which describes the driving force behind the crack propagation. The stress intensity factor increases with increasing external stress and the length of the crack. Furthermore, the size of the damage zone in front of the crack tip plays a decisive role. The size of the damage zone is largely dependent on the square of the ratio of the stress intensity factor to the yield point of the material and thus also increases with the crack length and stress amplitude. **Figure 9** shows a scheme of the damage zone for different crack lengths in LMCs. The size of the damage zone was calculated by the linear elastic fracture mechanics considering the different

Figure 8. Fatigue crack growth path of different samples (UFG Mono, homogeneous UFG LMC [Al/Al] and heterogeneous UFG LMC [Al/Steel]) that are representatively for the damage behavior in the LCF and HCF regimes.

Figure 9. Schematic representation of the interaction between the damage zone in front of the crack tip and the heterogeneous material interface and the resulting crack paths within the LMC for a) high stress amplitudes (LCF regime) and b) low stress amplitudes (HCF regime). Adapted with permission.[22] Copyright 2017, Elsevier.

material properties. Extensive plastic deformation occurs in front of the crack tip in the softer layer at a stress amplitude above the threshold stress (LCF regime), Figure 9a. However, further propagation of the damage zone is prevented as the crack approaches the material interface because of the significantly higher yield strength of the hard interlayer. This leads to an accumulation of deformation in front of the material interface within the softer layer. This was evidenced in the experiments by pronounced localized damage in form of a large number of secondary cracks in the softer layer near the material interface Figure 8b,c. In contrast, no secondary cracks are formed at a larger distance to the material interface along the main crack. Due to the continuously progressive crack, the local cumulative plastic deformation in this area is too low. Finally, these shielding mechanism in front of the material interface leads to crack branching and subsequent crack propagation within the softer layer approximately parallel to the material interface and loading direction. The crack propagation mechanisms in the LCF regime that were observed in this work are similar to those of CG lamellar metallic composites. This crack deflection at the material interface is attributed to a decrease in the effective driving force of crack propagation, as soon as the damage zone reaches the material interface.[20,21] If the applied stress is below the threshold stress (HCF regime), the size of the damage zone in front of the crack tip is relatively small, Figure 9b. Furthermore, both material layers are mainly elastically deformed during cyclic loading. As a result, there is only a little change in the damage zone at the material interface and the crack spreads very straight across the interface. These different macrocrack propagation mechanisms, which are present at high and low stress amplitudes, significantly influence the fatigue life in the LCF and HCF regimes.
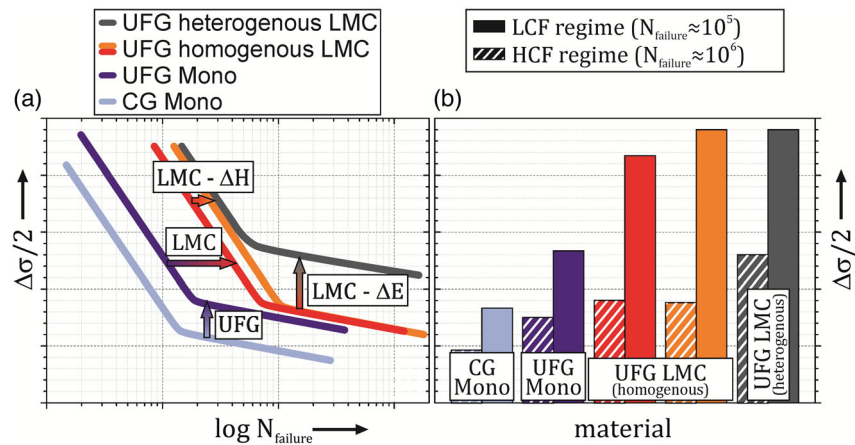
An influence of the interface affected zone (IAZ), which develops during the roll bonding process, on the observed cracking behavior can be neglected. The microstructural development

in the immediate vicinity of the material interface during ARB is very complex and depends on the processing parameters as well as on the used materials. A strongly enhanced grain refinement is found in a distance of around 50–200 nm at the material interface due to an additional plastic deformation in this area.[52] The main processing parameters that influence the microstructural development in the IAZ are the surface wire brushing before and the thickness reduction in each rolling step. These processing parameters were very similar for all the ARB sheets investigated. The only difference may come from the material combinations. For the homogenous LMCs, the elastic properties of the constituents are quite similar and the crystallographic system is identical. Therefore, a similar bonding mechanism and microstructural evolution is expected at the material interface in these LMCs. In contrast, for the heterogeneous aluminum/ steel LMCs, where materials with clearly distinct elastic and plastic mechanical properties and different crystallographic systems are combined, a larger IAZ is expected. However, the size of the plastic zone in front of the crack tip and the distance to the interface, where the crack deviation is observed, is significantly larger than the IAZ.

A detailed summary of the influence of the different material combinations and layer architectures in the LMCs is depicted schematically in a Wöhler *S–N* diagram in **Figure 10**a. Furthermore, Figure 10b shows the influence of the different material combinations and layer architectures in the LMCs on the fatigue strengths in the LCF and HCF regimes, respectively.

It is an open discussion whether or not the fatigue lives obey a rule of mixture. Fatigue failure is the consequence of a multistep process, starting with the localization of plastic deformation, the forming of microcracks, the evolution of these microcracks to a growable macrocrack, and the macrocrack propagation. Moreover, the portion of the individual steps on the total fatigue life varies with the applied stress, or, respectively, strain

Figure 10. Schematic Wöhler $S–N$ diagram ($\Delta\sigma/2/N_{failure}$) for monomaterial with CG and UFG sizes as well as for UFG LMCs. In addition, a differentiation was made between LMCs that are based on similar (homogenous) and nonsimilar (heterogeneous) materials to illustrate the influence of an increasing difference in the hardness (ΔH) or Young's modulus (ΔE) at the material interface. b) The fatigue limit ($\Delta\sigma/2$) of these different materials are shown that are representative for the fatigue strength in the LCF and HCF regimes ($N_{failure} \approx 10^5$ and 10^6), respectively.

amplitude. Thus, from a mechanistic point of view, assuming a rule of mixture is rather questionable and further investigations are needed to clarify this point. In this context, the particularities of a three-point-bending setup has to be regarded as well. Generally, the localization of plastic deformation is a prerequisite for the formation of a microcrack. Under three-point bending, the localization process is superimposed by the gradient in the bending moment and thus, the fatigue properties are strongly dependent on the outer material. The distinct influence of the outer layer is also illustrated, when we compare the portion of the total fatigue life that is necessary to initiate macrocrack propagation. While for the homogeneous LMCs, where always an AA1050 layer was at the outer side, 85–99% of the total fatigue life is needed to initiate the macrocrack, for the heterogeneous LMCs, where AA5005 is at the outer side, 75% of N_f are required.

The fatigue life is clearly enhanced at high stress amplitudes (LCF regime), if a high difference in hardness exists at the material interface. The gain in fatigue life increases with rising difference in hardness in both types of LMCs (homogenous and heterogeneous LMCs). This is a result of the more effective shielding of the damage zone and, associated therewith, an increasing crack deflection in front of the soft–hard material interface with an increasing difference in strength between the materials. The increase in fatigue life is significantly larger in the LMCs based on technically pure aluminum (Al–alloy1/Al–alloy2) compared with the Al/steel LMCs, that are based on either AA5005 or AA5754. This is a consequence of the lower yield strength in this material and, consequently, a significantly larger damage zone in front of the crack tip. Thus, the shielding effect is more pronounced at the material interface.

The gain in fatigue life at low stress amplitudes (HCF regime) can be explained by an increased resistance against the initiation of a macrocrack in the surface layer. This is achieved by two different mechanisms: The transformation from the CG microstructure into the UFG regime leads to a shift of the whole fatigue life curve to higher stress values, which is related to the higher strength of the UFG materials. As a result, micro

yielding phenomena, which are the starting point for material failure at low stress amplitudes, starts at considerably higher stress amplitudes in these materials. In the heterogeneous LMCs, a second mechanisms can occur, if a suitable material combination and layer architecture is used. In these LMCs, a stress redistribution into the inner, stiffer layers takes place resulting in a reduction of the tensile stresses at the surface.[49,50] This reduced stress in the outer layer increased the fatigue limit in the HCF regime to the same extent. By a suitable layer architecture in an aluminum/steel LMCs, it was possible to reduce the stress in the outer aluminum layer and increase the fatigue limit in the HCF regime by almost 30%.[50]

5. Conclusion

In this article, we aimed to clarify the influence of the grain size and of different layer architectures in homogenous and heterogeneous LMCs on the damage mechanisms and fatigue life under cyclic three-point bending. LMCs consisting of different aluminum alloys and of an aluminum alloy combined with a deep drawing steel were produced by ARB for this purpose. It was possible to systematically demonstrate the influence of an UFG structure and of the layer architecture of LMCs on the three-point-bending fatigue behavior by varying the processing parameters. Detailed microstructural investigations before and after the experiments revealed the material- and load-specific deformation and damage mechanisms. The results can be summarized to the following key points: 1) An increasing hardness due to an UFG structure leads to a shift of the fatigue life curve to higher stress amplitudes and therefore to an improvement in the fatigue life in the LCF and HCF regimes; 2) The hardness of the interlayer influences the fatigue life of LMCs only in the LCF regime. The fatigue life increases with rising difference in hardness at the material interface. In the HCF regime, the fatigue life is determined exclusively by the material behavior of the outer layer; 3) The fatigue life of heterogeneous LMCs, which have a high difference in hardness and Young's modulus at the

material interface, is significantly higher in both the LCF and HCF regimes than that of the reference monomaterial. This is due to a pronounced crack deflection at the soft-to-hard material interface (LCF regime) and to an effective load transfer into the stiffer, inner layers (HCF regime).

The significant increase in fatigue life of the UFG lamellar metallic composites is of great technological interest, as this improvement was achieved without increasing the density of the material. Furthermore, the crack propagation in the UFG composites was significantly slowed down. With a sufficiently high difference in strength and a near-surface layer of the stronger material, the crack propagation was even stopped at the material interface. This increases the safety of cyclically loaded components additionally, as a rapid crack growth can be excluded, that often leads to critical failure. Furthermore, a surface crack can be detected more easily and inexpensively. This results in an enormous potential for the use in cyclically loaded components. One example is the outer skin panels of aircrafts with their high importance of the weight-specific fatigue properties, as well as safety requirements.

Conflict of Interest

The authors declare no conflict of interest.

Data Availability Statement

Research data are not shared.

[1] J. Albert, *Arch. Miner. Geogn. Bergbau Hüttenkd.* **1838**, *10*, 215.

[2] A. Wöhler, *Z. Bauwesen* **1863**, *13*, 233.

[3] R. Woodward, *Mater. Des.* **1989**, *10*, 248.

[4] W. S. Miller, L. Zhuang, J. Bottema, A. J. Wittebrood, P. De Smet, A. Haszler, A. Vieregge, *Mater. Sci. Eng.: A* **2000**, *280*, 37.

[5] M. Nakai, T. Eto, *Mater. Sci. Eng.: A* **2000**, *285*, 62.

[6] T. Dursun, C. Soutis, *Mater. Des.* **2014**, *56*, 862.

[7] G. M. Scamans, N. Birbilis, R. G. Buchheit, *3.08 – Corrosion of Aluminum and its Alloys*, Elsevier, Oxford **2010**.

[8] R. Z. Valiev, R. K. Islamgaliev, I. V. Alexandrov, *Prog. Mater. Sci.* **2000**, *45*, 103.

[9] A. Azushima, R. Kopp, A. Korhonen, D. Y. Yang, F. Micari, G. D. Lahoti, P. Groche, J. Yanagimoto, N. Tsuji, A. Rosochowski, A. Yanagida, *CIRP Ann. Manuf. Technol.* **2008**, *57*, 716.

[10] Y. Estrin, A. Vinogradov, *Acta Mater.* **2013**, *61*, 782.

[11] S. R. Agnew, A. Y. Vinogradov, S. Hashimoto, J. R. Weertman, *J. Electron. Mater.* **1999**, *28*, 1038.

[12] H. Mughrabi, H. W. Höppel, M. Kautz, *Scr. Mater.* **2004**, *51*, 807.

[13] M. Goto, S. Z. Han, J. Kitamura, T. Yakushiji, J. H. Ahn, S. S. Kim, M. Baba, T. Yamamoto, J. Lee, *Int. J. Fatigue* **2015**, *73*, 98.

[14] M. V. Glazov, C. Laird, *Acta Metall. Mater.* **1995**, *43*, 2849.

[15] H. W. Höppel, Z. M. Zhou, H. Mughrabi, R. Z. Valiev, *Philos. Mag. A* **2002**, *82*, 1781.

[16] K. K. Chawla, P. K. Liaw, *J. Mater. Sci.* **1979**, *14*, 2143.

[17] J. Wittenauer, O. D. Sherby, *J. Eng. Mater. Technol.* **1987**, *109*, 244.

[18] S. Suresh, Y. Sugimura, E. K. Tschegg, *Scr. Metall. Mater.* **1992**, *27*, 1189.

[19] G. I. Bryzgalin, D. I. Tsvetkov, G. G. Kartashov, V. P. Nagibin, A. V. Pisarev, *Strength Mater.* **1989**, *21*, 1652.

[20] Y. Sugimura, P. G. Lim, C. F. Shih, S. Suresh, *Acta Metall. Mater.* **1995**, *43*, 1157.

[21] R. Pippan, K. Flechsig, F. O. Riemelmoser, *Mater. Sci. Eng.: A* **2000**, *283*, 225.

[22] F. Kümmel, H. W. Höppel, M. Göken, *Mater. Sci. Eng.: A* **2017**, *702*, 406.

[23] J. D. Pribe, T. Siegmund, J. J. Kruzic, *Eng. Fract. Mech.* **2020**, *235*, 107072.

[24] N. K. Simha, F. D. Fischer, O. Kolednik, C. R. Chen, *J. Mech. Phys. Solids* **2003**, *51*, 209.

[25] O. Kolednik, J. Predan, F. D. Fischer, P. Fratzl, *Adv. Funct. Mater.* **2011**, *21*, 3634.

[26] O. Kolednik, J. Predan, F. D. Fischer, P. Fratzl, *Acta Mater.* **2014**, *68*, 279.

[27] Y. Saito, N. Tsuji, H. Utsunomiya, T. Sakai, R. G. Hong, *Scr. Mater.* **1998**, *39*, 1221.

[28] M. Ruppert, W. Böhm, H. Nguyen, H. W. Höppel, M. Merklein, M. Göken, *J. Mater. Sci.* **2013**, *48*, 8377.

[29] M. Z. Quadir, O. Al-Buhamad, L. Bassman, M. Ferry, *Acta Mater.* **2007**, *55*, 5438.

[30] T. Hausöl, H. W. Höppel, M. Göken, *Mater. Sci. Forum* **2011**, *667–669*, 217.

[31] J. S. Carpenter, S. C. Vogel, J. E. LeDonne, D. L. Hammon, I. J. Beyerlein, N. A. Mara, *Acta Mater.* **2012**, *60*, 1576.

[32] S. Roy, B. R. Nataraj, S. Suwas, S. Kumar, K. Chattopadhyay, *Mater. Des.* **2012**, *36*, 529.

[33] F. Kümmel, M. Kreuz, T. Hausöl, H. W. Höppel, M. Göken, *Metals* **2016**, *6*, 56.

[34] M. Göken, H. W. Höppel, *Adv. Mater.* **2011**, *23*, 2663.

[35] V. Yousefi Mehr, M. R. Toroghinejad, A. Rezaeian, *Mater. Sci. Eng.: A* **2014**, *601*, 40.

[36] F. Kümmel, T. Hausöl, H. W. Höppel, M. Göken, *Acta Mater.* **2016**, *120*, 150.

[37] X. Ma, C. Huang, J. Moering, M. Ruppert, H. W. Höppel, M. Göken, J. Narayan, Y. Zhu, *Acta Mater.* **2016**, *116*, 43.

[38] F. Kümmel, T.-S. Tegtmeier, H. W. Höppel, M. Göken, *IOP Conf. Ser.: Mater. Sci. Eng.* **2017**, *194*, 012036.

[39] W. C. Oliver, G. M. Pharr, *J. Mater. Res.* **1992**, *7*, 1564.

[40] J. L. Hay, G. M. Pharr, *Instrumented Indentation Testing*, ASM International **2000**.

[41] H. W. Höppel, J. May, M. Göken, *Mater. Sci. Forum* **2008**, *584–586*, 840.

[42] X. Huang, N. Tsuji, N. Hansen, Y. Minamino, *Mater. Sci. Eng.: A* **2003**, *340*, 265.

[43] M. Eizadjou, H. D. Manesh, K. Janghorban, *J. Alloys Compd.* **2009**, *474*, 406.

[44] N. Tsuji, N. Kamikawa, B. Li, *Mater. Sci. Forum* **2007**, 2837.

[45] X. Molodova, G. Gottstein, M. Winning, R. J. Hellmig, *Mater. Sci. Eng.: A* **2007**, *460–461*, 204.

[46] J. May, M. Dinkel, D. Amberger, H. W. Höppel, M. Göken, *Metall. Mater. Trans. A* **2007**, *38*, 1941.

[47] H. W. Höppel, J. May, M. Göken, *Adv. Eng. Mater.* **2004**, *6*, 219.

[48] O. Engler, J. Aegerter, *Mater. Sci. Eng.: A* **2014**, *618*, 663.

[49] V. Luzin, S. Banovic, T. Gnäupel-Herold, H. Prask, R. E. Ricker, *Mater. Sci. Forum* **2005**, *495–497*, 1591.

[50] F. Kümmel, B. Diepold, A. Prakash, H. W. Höppel, M. Göken, *Int. J. Fatigue* **2018**, *116*, 379.

[51] F. Kümmel, B. Diepold, K. F. Sauer, C. Schunk, A. Prakash, H. W. Höppel, M. Göken, *Adv. Eng. Mater.* **2019**, *21*, 1800286.

[52] C. Schunk, M. Nitschky, H. W. Höppel, M. Göken, *Adv. Eng. Mater.* **2018**, *21*, 1800546.